



High-temperature flame spray pyrolysis induced stabilization of Pt single-atom catalysts

Shipeng Ding^a, Hsi-An Chen^b, Okorn Mekasuwandumrong^c, Max J. Hülsey^a, Xinpu Fu^a, Qian He^d, Joongjai Panpranot^{e,*}, Chia-Min Yang^{b,f,*}, Ning Yan^{a,*}

^a Department of Chemical and Biomolecular Engineering, National University of Singapore, 4 Engineering Drive 4, Singapore, 117585, Singapore

^b Department of Chemistry, National Tsing Hua University, Hsinchu, 30013, Taiwan

^c Department of Chemical Engineering, Faculty of Engineering and Industrial Technology, Silpakorn University, Nakorn Pathom, 73000, Thailand

^d Department of Materials Science and Engineering, National University of Singapore, 9 Engineering Drive 1, Singapore, 117575, Singapore

^e Center of Excellence on Catalysis and Catalytic Reaction, Biorefinery Cluster, Department of Chemical Engineering, Faculty of Engineering, Chulalongkorn University, Bangkok, 10330, Thailand

^f Frontier Research Center on Fundamental and Applied Sciences of Matters, National Tsing Hua University, Hsinchu, 30013, Taiwan

ARTICLE INFO

In deep memory of Prof. Maria Flytzani-Stephanopoulos, a pioneer and leader in single-atom catalysis among other subjects, and a great mentor to younger researchers in catalysis.

Keywords:

Flame spray pyrolysis
Single-atom catalysis
Thermal stability
CO oxidation
Methane combustion
Methane partial oxidation

ABSTRACT

Obtaining stable single-atom catalysts (SACs) for high-temperature applications remains challenging due to the thermodynamically favourable metal sintering under harsh reaction conditions. Taking advantage of the high-temperature process conditions (> 1000 °C), we hereby report the preparation of thermally stable metal oxide-supported single-atom Pt catalysts by flame spray pyrolysis. Among the four common supports (Al_2O_3 , SiO_2 , TiO_2 and ZrO_2) evaluated, single-atom Pt species were identified on Al_2O_3 , TiO_2 and ZrO_2 , among which ZrO_2 was the best to stabilize atomically dispersed Pt. Compared to single-atom Pt catalysts prepared through the conventional impregnation method, samples synthesized by flame spray pyrolysis displayed excellent catalytic performance in CO oxidation, methane combustion and methane partial oxidation reactions. Characterization results revealed that flame spray pyrolysis favoured the formation of tetragonal-monoclinic phase of ZrO_2 with improved redox property, thus leading to enhanced catalytic activity in high-temperature applications.

1. Introduction

Single-atom catalysts (SACs), featuring isolated metal atoms anchored onto a host, are of great interest in diverse applications [1–26]. However, the synthesis of stable SACs for high-temperature applications remains a challenge [17,27,28]. While conventional syntheses of SACs, such as coprecipitation [29–31], impregnation [32–35] and electrostatic adsorption [36,37], are typically performed below 600 °C, single-atom species on SACs fabricated at higher temperatures should inherently possess increased thermal stability. Several high-temperature SACs synthesis methods have been reported [29,38–44]. For example, a universal shockwave (1500–2000 K) method was developed to synthesize single-atom Pt, Ru and Co catalysts [39]. The high temperature process benefited the dispersion of metal atoms and promoted the formation of thermodynamically stable metal-defect bonds. This culminated in excellent catalyst stability when applied in CO oxidation and direct methane transformation to $\text{C}_2\text{-C}_6$ hydrocarbons. High-

temperature atom trapping was also demonstrated in preparing a sinter-resistant, atomically dispersed Pt/CeO₂ catalyst [40]. Pt atoms emitted from Pt nanoparticles (NPs) at 800 °C were captured and anchored in the most stable binding sites on CeO₂. Furthermore, the transformation of NPs to single-atom species at 900 °C was directly observed by in situ environment transmission electron microscopy [41].

Flame spray pyrolysis has been demonstrated to be an effective technique for synthesizing uniformly sized metal NPs [45–47]. Flame spray pyrolysis has a few advantages to prepare supported metal catalysts. First, the precursors are mixed in the solution, which allows the homogeneous mixing of all the precursors at atomic level in the starting phase [48]. Second, it is a single-step, cost-effective and scalable method to produce catalysts at kilogram scale per hour [49]. Third, the morphology and particle size of the catalysts can be effectively controlled by tuning the synthetic conditions [49]. Besides, the high combustion temperature, up to 1500–2000 °C, provides sufficient thermal energy to disperse and place metal atoms onto the most stable

* Corresponding authors.

E-mail addresses: joongjai.p@chula.ac.th (J. Panpranot), cmyang@mx.nthu.edu.tw (C.-M. Yang), ning.yan@nus.edu.sg (N. Yan).

<https://doi.org/10.1016/j.apcatb.2020.119471>

Received 14 May 2020; Received in revised form 12 August 2020; Accepted 22 August 2020

Available online 26 August 2020

0926-3373/ © 2020 Elsevier B.V. All rights reserved.

sites on the support. Fast quenching prevents the vaporization and recombination of metal atoms (Ostwald ripening), as well as the sintering of support due to overheating. NP catalysts prepared by flame spray pyrolysis have been widely applied in selective hydrogenation [50], methane combustion [51,52], selective oxidation of propylene [53], and propane dehydrogenation [54] in the temperature range from room temperature to 1000 °C. On the other hand, few examples of the high-temperature catalytic application of SACs synthesized by flame spray pyrolysis have been reported thus far. Two recent papers communicated the syntheses of single-atom Pd/TiO₂ catalyst using high-temperature flame spray pyrolysis, but these catalysts were only tested in solar light driven photocatalytic NOx removal [55,56]. Therefore, it could not be deduced whether flame spray pyrolysis is indeed a viable method to fabricate SACs for high temperature applications from the existing literature.

Herein, we attempted the synthesis of Pt SACs by flame spray pyrolysis (> 1000 °C) over a series of oxide supports. As revealed by Fourier transform infrared spectroscopy using CO as probe molecule and X-ray absorption spectroscopy (XAS), the dispersion of single atoms was highly dependent on the nature of the oxide support. Among the four common supports (Al₂O₃, SiO₂, TiO₂ and ZrO₂) examined, ZrO₂ was found to exert the strongest stabilization effect. In contrast with conventional wet impregnation method, flame spray pyrolysis processed Pt catalyst on ZrO₂ displayed superior catalytic performance in reactions such as CO oxidation (150–350 °C), methane combustion (400–700 °C) and methane partial oxidation (300–700 °C).

2. Methods

2.1. Synthesis of Pt catalysts

In flame spray pyrolysis, the combustion of the fuel gas produces high temperature, which could reach 1500–2000 °C depending on the processing conditions. The metalorganic precursor solution of the metal and support then is atomized into liquid droplets by the atomizer, and is transported to the flame zone with the help of the carrier gas. The transformation of the precursor solution into solid catalysts occurs via pyrolysis. Supported Pt catalysts were prepared using a flame reactor with platinum acetylacetonate (Pt(O₂C₅H₇)₂, Sigma-Aldrich, > 97.0 %), aluminium butoxide (Al[OCH(CH₃)C₂H₅]₃, Sigma-Aldrich, > 97.0 %), tetraethylorthosilicate (Si(OC₂H₅)₄, Sigma-Aldrich, > 97.0 %), titanium butoxide (Ti(OC₂H₅)₄, Sigma-Aldrich, > 97.0 %), and zirconium butoxide (Zr(OC₂H₅)₄, Sigma-Aldrich, 80.0 wt% in 1-butanol) as the starting precursors of Pt, Al, Si, Ti, and Zr, respectively. The desired amounts of each precursor were dissolved in xylene with a total precursor concentration (include both metal and support) of 0.5 M and a flow rate of 3 ml/min (denoted as condition 1). Pt doping content was fixed at 0.2 wt% in all samples. Mixture of precursors was injected through capillary of the gas-assist nozzle through a syringe pump at a flow rate of 3 mL/min. Methane and oxygen gas flow rate were adjusted to 1.5 L/min and 3 L/min, respectively. These gases served as fuel for the pre-mixed ignition flamelet and to support the spray flame. Oxygen disperse gas was adjusted to 5 L/min. The pressure drop across the nozzle was maintained at 1.5 bar. Thus obtained product was collected as powder using gas fiber filter with the aid of a vacuum pump. Two key parameters, including the total metal concentration and flow rate of the precursor solution, were varied for the synthesis of Pt/ZrO₂. Apart from condition 1 (concentration 0.5 M, flow rate 3 mL/min), two more conditions were tested (condition 2: concentration 0.3 M, flow rate 3 mL/min; condition 3: concentration 0.3 M, flow rate 2 mL/min). To disperse single-atom Pt on ZrO₂(m) or ZrO₂(t) using wet impregnation method, stoichiometric amounts of Pt(acac)₂ (0.1 wt%, compared to ZrO₂ support) was added to 5 ml of acetone and sonicated for 3 min. ZrO₂ was then added to the above solution and stirred for 12 h at room temperature. After the evaporation of the solvent, calcination was done at 200 °C in the air for 1 h to get the final catalyst.

2.2. Characterization of catalysts

High angle annular dark field scanning transmission electron microscopy (HAADF-STEM) were performed using an aberration-corrected JEOL ARM200CF microscope operated at 200 kV. Transmission electron microscopy (TEM) and scanning electron microscopy (SEM) images were recorded on a JEM 2100 F (JEOL) and on a JEM-6700 F (JEOL) microscope, respectively. N₂ adsorption–desorption isotherms were obtained on Quantachrome NOVA-3000 system at 77 K. Before the measurements, samples were degassed at 100 °C.

In situ diffuse reflectance infrared Fourier transform spectroscopy (in situ DRIFTS) study of CO chemisorption was performed on an FTIR spectrometer (Nicolet iS50) equipped with a mercury-cadmium-telluride (MCT) detector. After loading 30 mg samples into the high temperature chamber (Harrick equipped with ZnSn windows), pure N₂ at a flow rate of 40 ml/min was introduced to the chamber for one hour at room temperature. Subsequently, the background spectrum in the range of 2300–1800 cm⁻¹ was collected and automatically subtracted from the sample spectrum. Next, the samples were exposed to 5% CO in Ar (40 mL/min) for 1 h to reach the CO saturation coverage. N₂ was subsequently purged to remove the gaseous CO from the in situ cell and the final spectrum was collected with 64 scans at a resolution of 4 cm⁻¹. The H₂ temperature program reduction (H₂-TPR) profile of the supported Pt catalysts was conducted on a Builder PCSA-1000 instrument equipped with a thermal conductivity detector (TCD) to analyse the consumption of H₂. 30 mg of catalyst was loaded in a tube and the temperature of the sample was increased from room temperature to 550 °C in 5 vol. % H₂/Ar with a heating rate of 5 °C/min. H₂ titration was also performed on the Builder PCSA-1000 instrument. In a typical measurement, 60 mg of catalyst was pre-treated in pure air at 100 °C for 30 min, then successive doses of H₂ gas were introduced using N₂ as the carrier gas at 100 °C (400 μL of 5% H₂/N₂ per pulse).

X-ray photoemission spectroscopy (XPS) measurements were carried out at a UHV surface science endstation located at the wide-range beamline (TLS BL24A) of NSRRC. The details of the endstation can be found in the previous publication [57]. In brief, a PHOIBOS 150 energy analyzer (SPEC GmbH) in conjunction with an electron flood gun (5 eV, 70 μA) was used to acquire XPS data from the Pt/ZrO₂ samples. A low-energy X-ray (270 eV) was applied to enhance the detection of Pt 4f signals from the samples of very low Pt concentrations. The obtained values of binding energy were referenced to Zr 3d_{5/2} core level of ZrO₂, with a commonly accepted value of 183.2 eV. Despite of a careful implementation of charge neutralization, the spectral line shape was still subject to distortion and broadening to some degrees. With this limitation in mind, only the likely species present on the sample surfaces were extracted from spectral fitting.

The Pt L₃-edge XAS spectra were measured at beamlines BL17C1 and BL44A at NSRRC. The Pt samples and the bulk PtO₂ reference were measured in the fluorescence mode and the Pt foil was measured in the transmission mode. The X-ray absorption near-edge structure (XANES) and the extended X-ray absorption fine structure (EXAFS) were collected at room temperature. Three scans were acquired and averaged for each sample to improve the signal-to-noise ratio. ATHENA and ARTEMIS programs were used for XAS data analysis. Inductively coupled plasma-optical emission spectroscopy (ICP-OES) was conducted on iCAP 6000 to determine the Pt loading in prepared Pt/ZrO₂ samples. Pt/ZrO₂ catalysts were digested in aqua regia at 80 °C overnight, and the obtained solution was filtered and diluted prior to analysis. Wide-angle X-ray diffraction (XRD) analysis was conducted using a Bruker D8 Advance X-ray diffractometer. The data was collected in the range of 20–80° with a scan rate of 2°/min.

2.3. The activity measurement

All the oxidation reactions were performed in a laboratory assembled fixed-bed quartz tube reactor. The flow rate of gases was

controlled by mass flow controllers. The concentration of each gas was determined by an Agilent 7890B gas chromatography (GC) equipped with a thermal conductivity detector (TCD). In each measurement, 30 mg of catalyst was placed between quartz wool and loaded in the middle of the reactor. For the CO oxidation activity measurement, a gas mixture (60 mL/min) containing 2.5 % O₂ and 2.5 % CO balanced with Ar was introduced to the quartz tube. The quartz tube was heated to the desired temperature for 30 min to reach steady state. Subsequently, the concentration of CO and CO₂ were recorded to determine the CO conversion. In the case of methane combustion, the feed gas of 0.25 % methane and 4.75 % O₂ (Ar balance) passed through the catalyst at a flow rate of 80 mL/min. The reaction temperature was increased from 200 to 700 °C at a temperature interval of 50 °C, and the gas species were measured when the steady state was reached after waiting for 30 min at each temperature. For methane partial oxidation, the feed gas contained 3.33 % methane, 1.67 % O₂ and balance Ar with a total flow rate of 30 mL/min. The catalytic performance was tested in the temperature range of 300–700 °C. The methane conversion and H₂(CO, CO₂) selectivity are defined as below:

$$CH_4 \text{ Conversion} (\%) = \frac{[CH_4]_{in} - [CH_4]_{out}}{[CH_4]_{in}} \times 100\%$$

$$H_2 \text{ Selectivity} (\%) = \frac{[H_2]_{out}}{2[CH_4]_{in} - 2[CH_4]_{out}} \times 100\%$$

$$CO \text{ Selectivity} (\%) = \frac{[CO]_{out}}{[CH_4]_{in} - [CH_4]_{out}} \times 100\%$$

$$CO_2 \text{ Selectivity} (\%) = \frac{[CO_2]_{out}}{[CH_4]_{in} - [CH_4]_{out}} \times 100\%$$

Where $[CH_4]_{in}$ represents the concentration of methane before the reaction, while $[CH_4]_{out}$, $[H_2]_{out}$, $[CO]_{out}$, and $[CO_2]_{out}$ indicate the concentration of methane, H₂, CO and CO₂ after the reaction, respectively.

3. Results and discussion

3.1. Preparation of metal oxide-supported Pt catalysts by flame spray pyrolysis

The loadings of Pt in the catalysts with ZrO₂, TiO₂, SiO₂ and Al₂O₃ as supports were determined to be around 0.2 wt% by ICP-OES. As such, the freshly prepared catalysts were denoted as 0.2 Pt/ZrO₂, 0.2 Pt/TiO₂, 0.2 Pt/SiO₂ and 0.2 Pt/Al₂O₃, respectively. The morphology of the as prepared catalysts was examined by SEM and TEM. The average size of metal oxide supports was around 20 nm (Fig. S1), while no obvious Pt nanoparticles were identified in the low resolution TEM images (Fig. S2).

The oxidation state and coordination environment of Pt were revealed by XAS at the Pt L₃-edge. As depicted in Fig. 1A, the normalized XANES spectra of 0.2 Pt/TiO₂ and 0.2 Pt/ZrO₂ resembled that of bulk PtO₂, while the spectra of 0.2 Pt/Al₂O₃ and 0.2 Pt/SiO₂ were almost overlapped with that of Pt foil. From these, the oxidation state of Pt in 0.2 Pt/TiO₂ and 0.2 Pt/ZrO₂ might be 4+, while Pt in 0.2 Pt/Al₂O₃ and 0.2 Pt/SiO₂ was fully reduced. The Fourier-transform (FT) profiles of the k³-weighted EXAFS and corresponding fitted results (e.g. interatomic distance (R) and coordination number (CN)) are shown in Fig. 1B, Fig. S3 and Tab. S1. The samples 0.2 Pt/Al₂O₃ and 0.2 Pt/SiO₂ showed a strong first-shell peak corresponding well to the Pt-Pt coordination of metallic Pt ($R_{Pt-Pt} = 2.76$ Å, $CN_{Pt-Pt} = 7.4$ and 8.1 for 0.2 Pt/Al₂O₃ and 0.2 Pt/SiO₂, respectively). The sizes of the Pt NPs in the two samples were around 1.3 nm, estimated from the Pt-Pt coordination number based on face-centered cubic Pt structure and a spherical model [58,59]. On the other hand, a dominant first-shell peak at 1.99 Å corresponding to the Pt-O bonding was observed for 0.2 Pt/TiO₂ and 0.2 Pt/ZrO₂ [31]. The fitted values of Pt-O coordination number for 0.2 Pt/TiO₂ and 0.2 Pt/ZrO₂ were close to 4, suggesting that the properties

of TiO₂ and ZrO₂ seemed to play a determining role in dispersing and anchoring isolated Pt atoms.

Using 0.2 Pt/ZrO₂ as an example, the effects of synthetic conditions on the formation of single-atom Pt were investigated. Under normal conditions, a higher flow rate of the precursor solution leads to a higher pyrolysis temperature, [56] increased flame height, and longer residence time in flame, whereas less concentrated precursor solution would result in the formation of smaller sized particles. The white line intensity of all 0.2 Pt/ZrO₂ samples in the XANES spectra (Fig. S4A) was similar, and all Pt samples showed a dominant Pt-O contribution in the FT profiles of the EXAFS spectra (Figs. S3C and S4B). These results indicated that the flame spray pyrolysis technique enabled the formation of isolated Pt on ZrO₂ over a broad range of synthetic conditions. Furthermore, the Pt-O coordination structure was also modulated by varying the flow rate and concentration of the precursor solution. For example, when the concentration of the precursor solution was increased from 0.3 to 0.5 mol/L, the Pt-O coordination number was tuned from 5.2 to 4.3. As the coordination structure plays an important role in determining the properties of SACs [60,61], it is expected that the catalytic performance of the SACs prepared by flame spray pyrolysis could be optimized by varying the synthetic conditions.

The dispersion of Pt atoms on ZrO₂, TiO₂, SiO₂ and Al₂O₃ was further examined by CO adsorption using in situ DRIFTS technique. As shown in Fig. 1C, the as-prepared 0.2 Pt/SiO₂ showed one peak at 2079 cm⁻¹. This signal is assigned to linearly adsorbed CO on metallic Pt atoms, indicating the dominant formation of Pt NPs on SiO₂. The CO adsorption peak at around 2090 cm⁻¹ is assignable to linear CO adsorption on positively charged Pt species. The broad CO signal between 2090–2020 cm⁻¹, observed for 0.2 Pt/Al₂O₃, 0.2 Pt/ZrO₂ and 0.2 Pt/TiO₂ catalysts, indicates that both positively charged and metallic Pt species are present [16,62]. Both EXAFS (Fig. 1B) and CO-DRIFTS (Fig. 1C) techniques consistently suggest that 0.2 Pt/ZrO₂ possessed the highest percentage of single-atom Pt among the four supports. Nevertheless, CO-DRIFTS spectrum indicated the presence of a small amount of Pt NPs co-existing with Pt single-atom on the surface of 0.2 Pt/ZrO₂, but no Pt-Pt shell was identified in the EXAFS spectrum. This inconsistency is attributed to the different operating principles of the two characterization techniques. DRIFTS is a surface sensitive analysis technique whereas XAS elucidates the averaged bulk structural information with an error of 10–20 % with regards to the coordination environment [63].

From above, we proved that high temperature flame spray pyrolysis is a viable technique for the formation of single-atom Pt species across a range of metal oxide supports. The stabilization of single-atom Pt is highly dependent on support type, with ZrO₂ being most effective. As confirmed by the HAADF-STEM images in Fig. 2 (vide infra), the isolated Pt atoms are embedded into the matrix of ZrO₂ by occupying Zr⁴⁺ positions during the high temperature synthesis process. Similar result was reported by Li, Sautet and co-workers that the most stable configuration for single-atom Rh on TiO₂ catalyst was the substitutional structure in which Rh replaced Ti under calcination conditions [36]. In our study, the EXAFS show that the density of single-atom Pt is much higher on ZrO₂ and TiO₂ than on Al₂O₃ and SiO₂, which can be rationalized by the relative size of Pt⁴⁺ and the size of the cation in the oxide support. The ionic radius is 86, 74.5, 67.5 and 54 pm for Zr⁴⁺, Ti⁴⁺, Al³⁺ and Si⁴⁺, respectively, while that number is 76.5 pm for Pt⁴⁺ and 94 pm for Pt²⁺ [64]. During flame spray synthesis, the substitution of support cation by Pt cation is easier to occur on TiO₂ and ZrO₂ considering their comparable cation radius and coordination requirements [65].

To evaluate the catalytic performance of single-atom Pt species without the interference from co-existing Pt NPs, 0.2 Pt/ZrO₂ was treated in sodium cyanide (NaCN). This method is widely adopted in the mining industry for the extraction of Au, Ag and other noble metals from primary ores [66]. Flytzani-Stephanopoulos and others have also demonstrated this method to be efficient in the selective removal of Pt

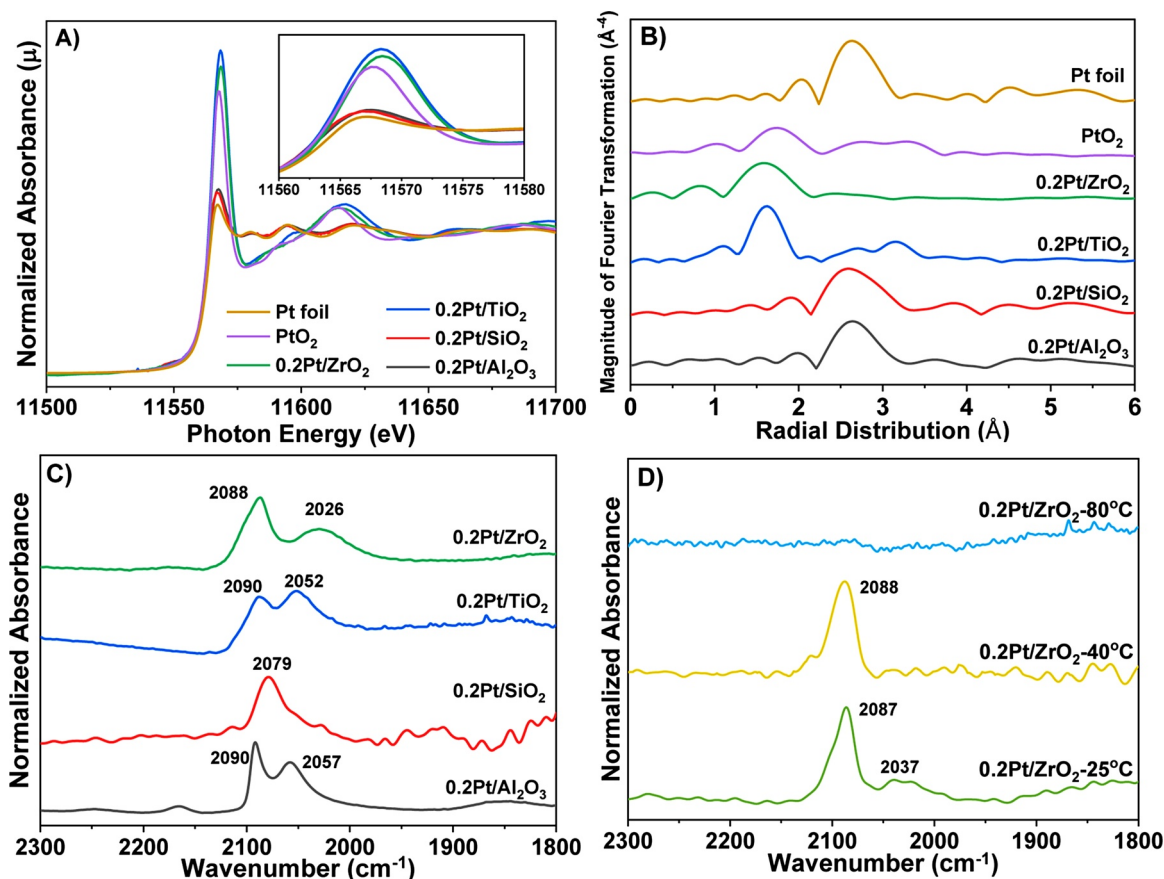


Fig. 1. (A) The normalized Pt L_{3} -edge XANES and (B) the FT profiles of k^3 -weighted EXAFS of the Pt catalysts prepared by flame spray pyrolysis (0.2 Pt/ZrO₂, 0.2 Pt/TiO₂, 0.2 Pt/SiO₂ and 0.2 Pt/Al₂O₃) and reference samples of Pt foil and PtO₂. The range of k for Fourier transformation was 3.9–10.9 Å⁻¹. (C) In situ DRIFTS of CO adsorption on freshly prepared Pt samples. (D) In situ CO adsorption on 0.2 Pt/ZrO₂ that was washed by NaCN solution at different temperatures for 12 h.

and Au NPs from a mixture of single-atom species and NPs on oxide supports [67–69]. The leaching was conducted in 2.0 wt% NaCN solution under pH 12 at three different temperatures—room temperature, 40 °C and 80 °C. In situ DRIFTS of CO adsorption was performed to examine the state of Pt species on the support post leaching. As exhibited in Fig. 1D, the CO adsorption intensity on metallic Pt decreased significantly after NaCN treatment at room temperature for 12 h compared with untreated Pt/ZrO₂ (Fig. 1C), indicating the effectiveness of the method to remove Pt NPs. Raising leaching temperature to 40 °C lead to observation of CO binding solely on atomically dispersed Pt. Further increasing the temperature to 80 °C resulted in the disappearance of CO adsorption signals on either Pt single-atom or NPs. This is likely due to the complete removal of Pt species from ZrO₂ under harsh leaching conditions. The mass loading of Pt in Pt/ZrO₂ after NaCN leaching at 40 °C was determined to be 0.1 wt.% by ICP-OES. This particular sample was denoted as 0.1Pt₁/ZrO₂-flame for further analyses.

The 0.1 Pt₁/ZrO₂-flame catalyst was characterised by aberration-corrected STEM. Representative high angle annular dark field (HAADF) images are shown in Fig. 2. As expected, no Pt nanoparticles were found in the catalyst (Fig. 2A and S5). While Pt clusters around 1 nm can be found occasionally (Fig. 2B), the vast majority of Pt species are atomically dispersed (as highlighted with circles in Fig. 2C–D). Fig. 2C and D, which show monoclinic ZrO₂ particles viewed from near [110] and [553] respectively, [70–72] indicate that Pt atoms exclusively sit on Zr sites. The dispersion of Pt for the 0.1 Pt₁/ZrO₂-flame sample was examined by H₂ titration at 100 °C (Fig. S6). No obvious H₂ uptake was observed, probably as a result of the weak H₂ adsorption ability of the 0.1Pt₁/ZrO₂-flame sample. The Pt-O bond was the only identifiable coordination shell as shown in EXAFS (Fig. S7A). XANES indicated that

the oxidation state of 0.1Pt₁/ZrO₂-flame was close to that of PtO₂ (Fig. S7B), while the CO absorption on Pt atoms suggested a 2+ oxidation state (Fig. 1D). This inconsistency was likely due to the reduction of Pt species from 4+ to 2+ during the CO adsorption. Similar phenomena was observed on single-atom Rh catalyst in which Rh³⁺ was reduced to Rh⁺ during CO treatment [73].

Fig. 3A illustrates the XRD pattern of 0.1Pt₁/ZrO₂-flame. Distinct diffraction peaks assignable to tetragonal and monoclinic ZrO₂ were identified, indicating the formation of tetragonal-monoclinic mixed phase. Based on this, single Pt atoms dispersed on both tetragonal and monoclinic ZrO₂ were fabricated by wet impregnation as control samples to contrast the advantages of single-atom Pt forged by flame spray pyrolysis. The Pt mass loading was controlled as 0.1 wt%, and the obtained samples were denoted as 0.1Pt₁/ZrO₂(m)-wet (m stands for monoclinic) and 0.1Pt₁/ZrO₂(t)-wet (t stands for tetragonal), respectively. The dominant existence of single-atom Pt was verified by CO adsorption, which showed only one sharp peak at 2089 cm⁻¹ that was assigned to linearly adsorbed CO on atomically dispersed Pt species (Fig. 3B). The isolated Pt atoms were found on the Zr sites by HAADF-STEM (Fig. S8), in consistent with the literature report in which single Pt atoms replaces the native oxide cation through wet impregnation approaches [74,75]. The XRD pattern of 0.1Pt₁/ZrO₂(m)-wet and 0.1Pt₁/ZrO₂(t)-wet samples showed diffraction of ZrO₂(m) and ZrO₂(t) without discernible Pt peak (Fig. 3A). The N₂ adsorption/desorption isotherms and BET surface area were displayed in Fig. S9. The 0.1Pt₁/ZrO₂-flame sample showed a lower surface area of 66 m²/g, likely due to the formation of tetragonal-monoclinic ZrO₂ with high crystallinity under high temperature.

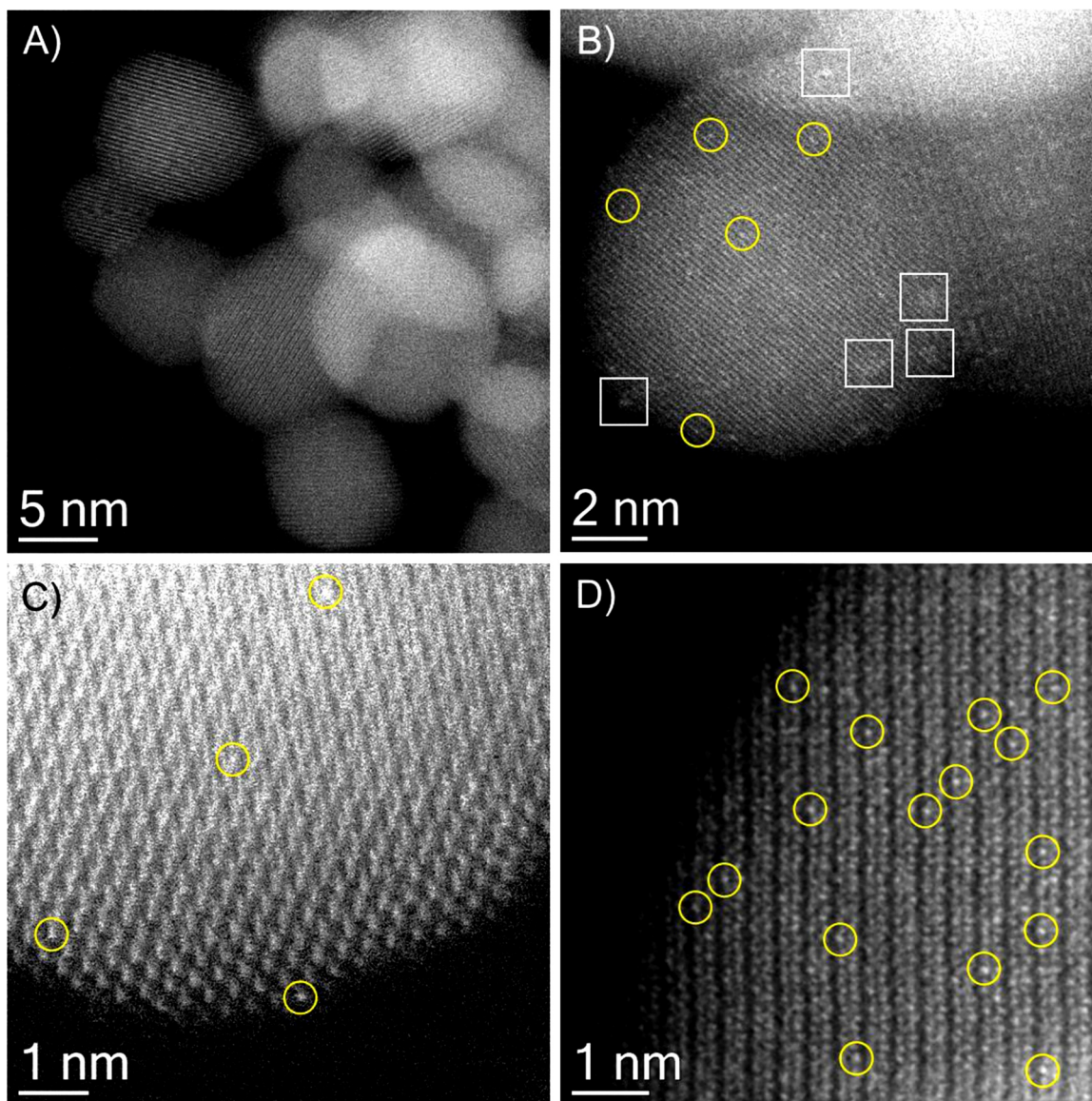


Fig. 2. Representative STEM-HAADF images of the 0.1Pt₁/ZrO₂-flame catalyst. (A) The low resolution TEM image. Pt clusters with size around 1 nm are highlighted by white squares in (B). Atomically dispersed Pt species are highlighted with yellow circles. Images in (C) and (D) show monoclinic ZrO₂(m) particles oriented close to the [110] and the [553] zone, respectively, indicating that Pt atoms are located at Zr sites. (For interpretation of the references to colour in this figure legend, the reader is referred to the web version of this article).

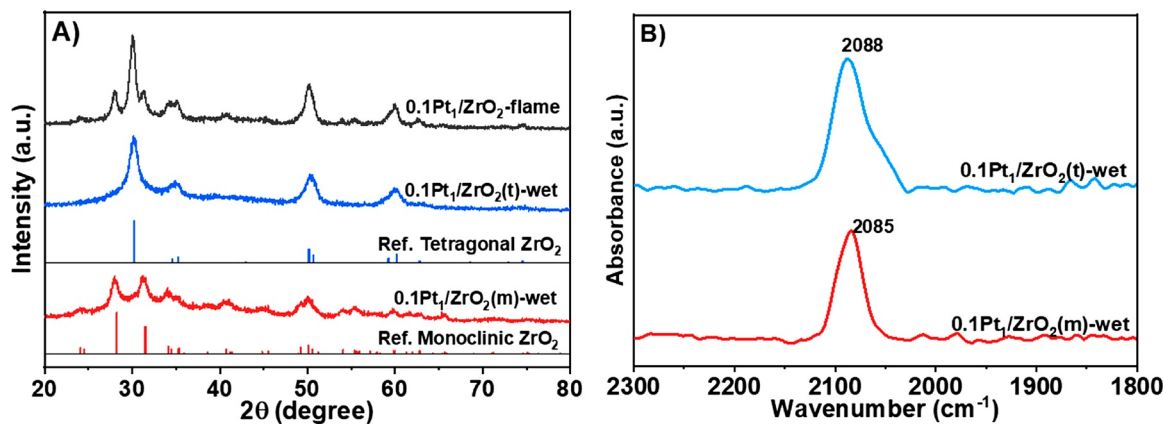


Fig. 3. (A) XRD pattern of single-atom 0.1Pt₁/ZrO₂-flame, 0.1Pt₁/ZrO₂(t)-wet, 0.1Pt₁/ZrO₂(m)-wet and reference tetragonal/monoclinic ZrO₂. (B) CO adsorption on 0.1Pt₁/ZrO₂(t)-wet and 0.1Pt₁/ZrO₂(m)-wet.

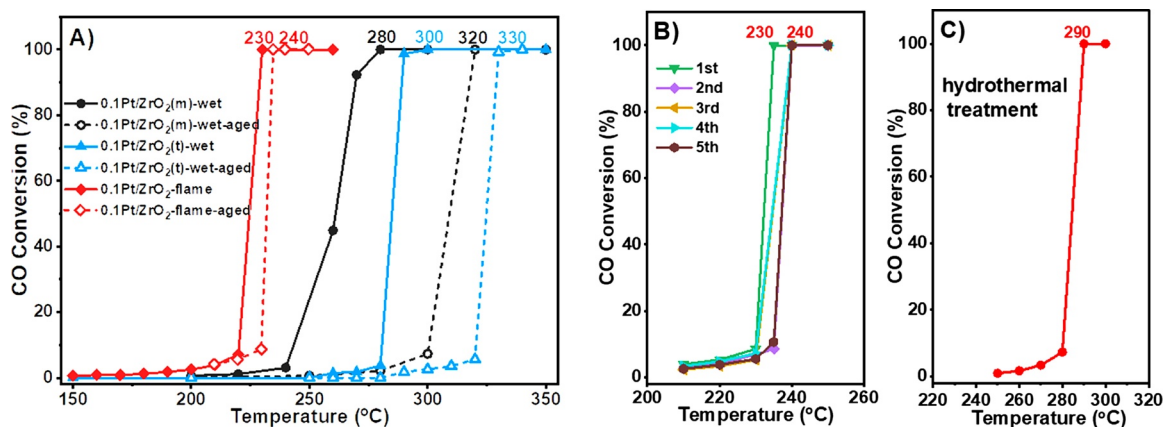


Fig. 4. (A) CO conversion as a function of temperature from 150 to 350 °C over 0.1Pt₁/ZrO₂-flame, 0.1Pt₁/ZrO₂(t)-wet and 0.1Pt₁/ZrO₂(m)-wet before and after thermal aging in 5% O₂/Ar at 700 °C for 12 h. (B) The recyclability test of 0.1Pt₁/ZrO₂-flame in CO oxidation. (C) The CO oxidation performance of 0.1Pt₁/ZrO₂-flame after thermal aging in 10 % H₂O at 700 °C for 12 h. Reaction conditions: 2.5 % O₂, 2.5 % CO balanced with Ar, 60 mL/min, 30 mg catalyst.

3.2. The catalytic performance of single-atom 0.1Pt₁/ZrO₂ in CO oxidation

Catalytic CO oxidation to CO₂ is an industrially relevant reaction in the removal of CO from H₂ rich atmosphere in fuel cell applications and CO elimination from automobile exhaust [40]. The CO oxidation catalysts used in diesel exhaust treatment system typically suffer from severe thermal deactivation due to the sintering of active species at high temperatures. The exhaust temperature may reach up to 750 °C during the regeneration process of diesel particulate filter [76]. In addition, the engine exhaust usually contains discrete amounts of water vapor, which negatively impacts the performance of oxidation catalysts. Thus, enduring thermal and hydrothermal stability of the CO oxidation catalyst are desirable properties in practical applications [77]. SACs have been reported to shown excellent activity in CO oxidation [73,78–80]. However, there are limited studies on the stability of SACs in CO oxidation reactions [40,62,81].

Fig. 4A shows the CO oxidation light-off curve on single-atom Pt₁/ZrO₂ catalysts before and after 700 °C thermal aging. The T₁₀₀ (temperature at which 100 % CO conversion occurred) on freshly prepared 0.1Pt₁/ZrO₂-flame, 0.1Pt₁/ZrO₂(m)-wet and 0.1Pt₁/ZrO₂(t)-wet was 230, 280 and 300 °C, respectively. The 0.1Pt₁/ZrO₂-flame sample displayed much higher activity than 0.1Pt₁/ZrO₂(m)-wet and 0.1Pt₁/ZrO₂(t)-wet samples. To gain insight into the activity difference of 0.1Pt₁/ZrO₂(m)-wet, 0.1Pt₁/ZrO₂(t)-wet and 0.1Pt₁/ZrO₂-flame, H₂-TPR was carried out and the results are shown in Fig. 5. All the catalysts displayed two reduction peaks. The peak at lower temperature was assigned to the reduction of surface active oxygen species neighbouring the Pt atoms, while the peak at higher temperature was ascribed to the reduction of monoclinic or tetragonal phases of ZrO₂ [82]. Apparently, the redox ability of the catalysts followed the order of 0.1Pt₁/ZrO₂-flame > 0.1Pt₁/ZrO₂(m)-wet, 0.1Pt₁/ZrO₂(t)-wet, which was consistent with the catalytic performance of the three catalysts in CO oxidation. Compared with SAC Pt₁/ZrO₂ prepared by wet impregnation, the flame spray pyrolysis prepared Pt₁/ZrO₂ showed better redox ability, thus rationalizing its higher catalytic performance in oxidation reactions.

Further, the three samples were then subjected to thermal aging at 700 °C for 12 h, after which the T₁₀₀ only slightly increased 10 °C from 230 to 240 °C for 0.1Pt₁/ZrO₂-flame, but increased more prominently at 40 °C for 0.1Pt₁/ZrO₂(m)-wet and 30 °C for 0.1Pt₁/ZrO₂(t)-wet. The durability of 0.1Pt₁/ZrO₂-flame was also examined. As shown in Fig. 4B, no discernible deactivation was observed in 5 cycles, with T₁₀₀ holding constant at 230–240 °C. Subjecting 0.1Pt₁/ZrO₂-flame to hydrothermal aging at 700 °C for 12 h resulted in a T₁₀₀ value of 290 °C (Fig. 4C), which was still lower than that of thermally treated 0.1Pt₁/ZrO₂(t) and 0.1Pt₁/ZrO₂(m) at 700 °C. These data reveal the excellent hydrothermal stability of single-atom Pt/ZrO₂ fabricated by flame spray

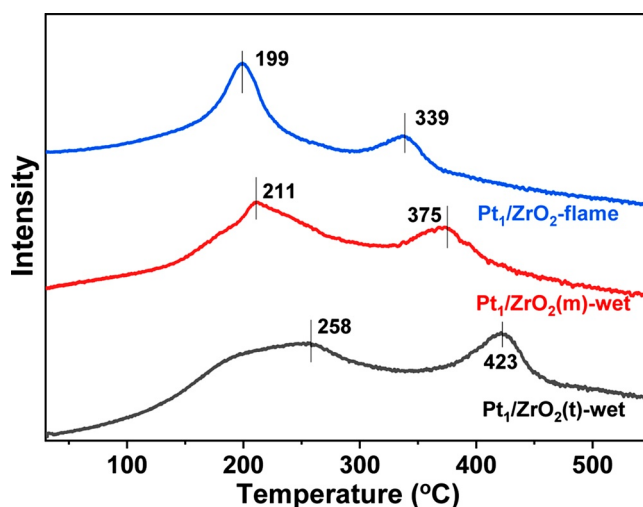


Fig. 5. H₂-TPR profiles of the 0.1Pt₁/ZrO₂-flame, 0.1Pt₁/ZrO₂(m)-wet and 0.1Pt₁/ZrO₂(t)-wet.

pyrolysis.

3.3. The catalytic performance of single-atom 0.1Pt₁/ZrO₂ in methane combustion

Methane is regarded as a promising clean energy source and has been widely used in various industrial applications such as natural gas vehicles, gas turbine and fuel cells [83–87]. The direct methane combustion conventionally occurs at above 1200 °C, thermodynamically favouring the formation of undesired CO and NO_x pollutants [88]. Catalytic methane combustion is able to reduce pollution emission, improve methane utilization efficiency, and lead to a lower light-off temperature [88]. The reaction activation energy was decreased from 100–200 kJ/mol for direct methane combustion to 40–80 kJ/mol for catalytic combustion [85].

Catalytic methane combustion over single-atom 0.1Pt₁/ZrO₂-flame was investigated in 0.25 % methane and 4.75 % O₂. For comparison purposes, 0.1Pt₁/ZrO₂(m)-wet and commercial 5% Pt/Al₂O₃ were also tested. 0.1Pt₁/ZrO₂(t)-wet was omitted as ZrO₂(t) was thermodynamically less stable than ZrO₂(m) [89], and 0.1Pt₁/ZrO₂(t)-wet displayed poor activity in CO oxidation earlier. As exhibited in Fig. 6A, single-atom 0.1Pt₁/ZrO₂-flame showed better methane combustion activity compared to commercial 5%Pt/Al₂O₃ and single-atom 0.1Pt₁/ZrO₂(m)-wet. The methane conversion at 450 °C for 0.1Pt₁/ZrO₂-flame

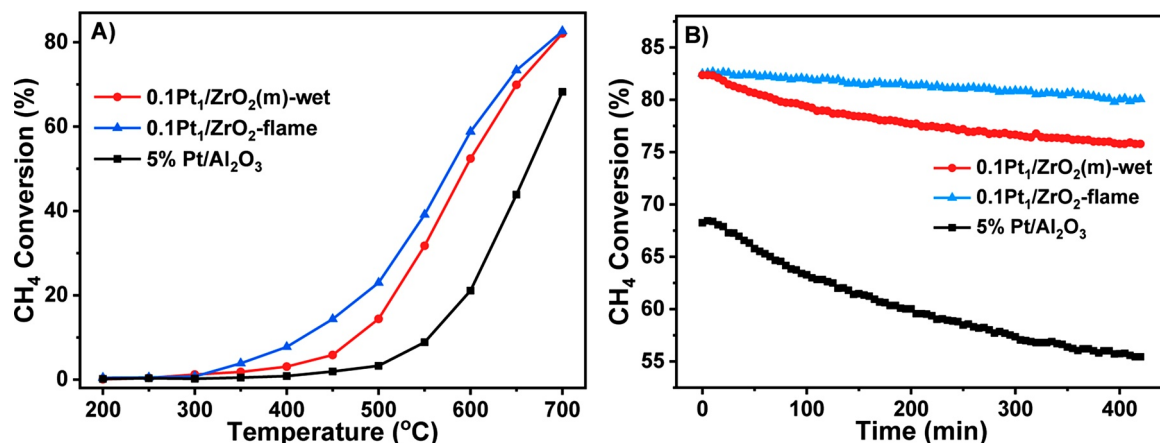


Fig. 6. (A) The catalytic performance as a function of temperature and (B) the long-term stability test at 700 °C for 0.1Pt₁/ZrO₂-flame, 0.1Pt₁/ZrO₂(m)-wet and commercial 5%Pt/Al₂O₃ in methane combustion. Reaction conditions: 0.25 % methane, 4.75 % O₂, 80 mL/min, 30 mg of 0.1Pt₁/ZrO₂-flame and 0.1Pt₁/ZrO₂(m)-wet. To keep the total amount of Pt the same for better comparison, Al₂O₃ was used to dilute the commercial 5% Pt/Al₂O₃.

was 14.5 %, which was about 2.5 times higher than 0.1Pt₁/ZrO₂(m)-wet (5.8 %). The specific activity of the 0.1Pt₁/ZrO₂-flame at 700 °C was 12.1 mol_{methane} h⁻¹ g_{Pt}⁻¹, much higher than the reported single-atom Pt₁/FeO_x (2.01 mol_{methane} h⁻¹ g_{Pt}⁻¹) under similar reaction conditions [29]. The activation energy was also determined while keeping methane conversion below 10 % (Fig. S10). The values were 66.9 and 48.9 kJ/mol for 0.1Pt₁/ZrO₂(m)-wet and 0.1Pt₁/ZrO₂-flame, respectively.

The long-term durability was also investigated at 700 °C, at which both 0.1Pt₁/ZrO₂-flame and 0.1Pt₁/ZrO₂(m)-wet showed a similar initial conversion of 82 %. The methane conversion over 0.1Pt₁/ZrO₂-flame decreased only marginally from 82 % to 80 % after 7 h. A more noticeable decrease from 82 % to 71 % on 0.1Pt₁/ZrO₂(m)-wet was identified after the same duration. The commercial 5% Pt/Al₂O₃ exhibited even faster deactivation, during which the conversion dropped from 67 % to 50 %. To quantify the deactivation rate of Pt catalysts, a typical first-order deactivation model was assumed and the deactivation constant k_d was determined by the equation

$$k_d = \frac{\ln[(1 - X_{final})/X_{final}] - \ln[(1 - X_{initial})/X_{initial}]}{t} \times 100\%$$

where t means the reaction time, and X_{final} and $X_{initial}$ represent the final and initial methane conversion, respectively [90]. The deactivation constant was 0.02 h⁻¹ for 0.1Pt₁/ZrO₂-flame, 0.06 h⁻¹ for 0.1Pt₁/ZrO₂(m)-wet and 0.08 h⁻¹ for commercial 5%Pt/Al₂O₃. Among the three samples investigated, 0.1Pt₁/ZrO₂-flame displayed the lowest deactivation rate and the highest catalytic activity, verifying the benefits of SACs formation by high temperature flame pyrolysis. The electronic property of Pt in the 0.1Pt₁/TiO₂-flame before and after methane combustion at 700 °C was surveyed by XPS. As shown in Fig. S11, the Pt_{4f} XPS peaks of the as-prepared 0.1Pt₁/ZrO₂-flame consist of two pairs of doublets: the doublet at higher and lower binding energy is assigned to Pt⁴⁺ and Pt²⁺, respectively. The dominant Pt species in the freshly prepared 0.1Pt₁/ZrO₂-flame sample was Pt²⁺. After methane combustion at 700 °C, the Pt species in the spent 0.1Pt₁/ZrO₂-flame were still in high oxidation state and the fraction of Pt²⁺ was decreased, as a result of the oxidation of Pt²⁺ to Pt⁴⁺ in high-temperature oxidation atmosphere (Fig. S11). The structure of the spent 0.1Pt₁/ZrO₂-flame catalyst was further examined by CO adsorption and HAADF-STEM, both of which proved that Pt species were still atomically dispersed after reaction (Fig. S12 and S13).

3.4. The catalytic performance of single-atom 0.1Pt₁/ZrO₂ in methane partial oxidation to syngas gas

Syngas production from methane has been receiving much attention in recent years [91,92]. However, research on methane partial oxidation over SACs has been limited. Thus, the performance of 0.1Pt₁/ZrO₂-flame and 0.1Pt₁/ZrO₂(m)-wet in the reaction was investigated in the range of 300–700 °C. As shown in Fig. 7 A–C, 0.1Pt₁/ZrO₂-flame sample exhibits better methane conversion, H₂ selectivity and CO selectivity than 0.1Pt₁/ZrO₂(m)-wet. Methane conversion and H₂ selectivity on 0.1Pt₁/ZrO₂-flame reached around 40 % and 70 %, respectively at 550 °C. In the case of 0.1Pt₁/ZrO₂(m)-wet, no formation of H₂ and CO was detected below 550 °C. Instead, methane was predominantly transformed to CO₂ or carbon. Much less CO₂ was formed on 0.1Pt₁/ZrO₂-flame compared to 0.1Pt₁/ZrO₂(m)-wet above 450 °C (Fig. 7D). With regards to durability at 700 °C, 0.1Pt₁/ZrO₂-flame maintained the methane conversion rates and selectivity towards H₂ and CO for over 40 h (Fig. 8). The dispersion of 0.1Pt₁/ZrO₂-flame after long term stability test was examined by CO adsorption. As shown in Fig. S14, apart from the CO adsorption on single-atom Pt at 2082 cm⁻¹, a small shoulder peak at around 2050 cm⁻¹ that was assigned to CO adsorption on Pt nanoparticles was also identified. Those results indicate that a majority of single-atom Pt survived the stability test in methane partial oxidation despite the H₂ generated in the system is well known to induce the aggregation of single atoms.

4. Conclusions

In summary, we prepared and characterized single-atom Pt catalysts on several oxide supports via flame spray pyrolysis. The effectiveness of the method is dependent on the nature of supports with ZrO₂ showing the best stabilization effect. The isolated Pt species were confined into the matrix of ZrO₂ through substituting the Zr cations during the flame spray pyrolysis process. In contrast with impregnation synthesized SAC 0.1Pt₁/ZrO₂, the flame spray prepared catalyst with the same Pt content exhibited a mixed tetragonal-monoclinic ZrO₂ support phase with improved redox ability, thus enabling considerably enhanced high-temperature catalytic performance in CO oxidation, methane combustion and methane partial oxidation. This study shows that flame spray pyrolysis is a promising and potentially general method to produce thermally stable SACs for a range of reactions.

Author credit statement

N.Y. conceived and supervised the project. J.P. and C.Y. co-

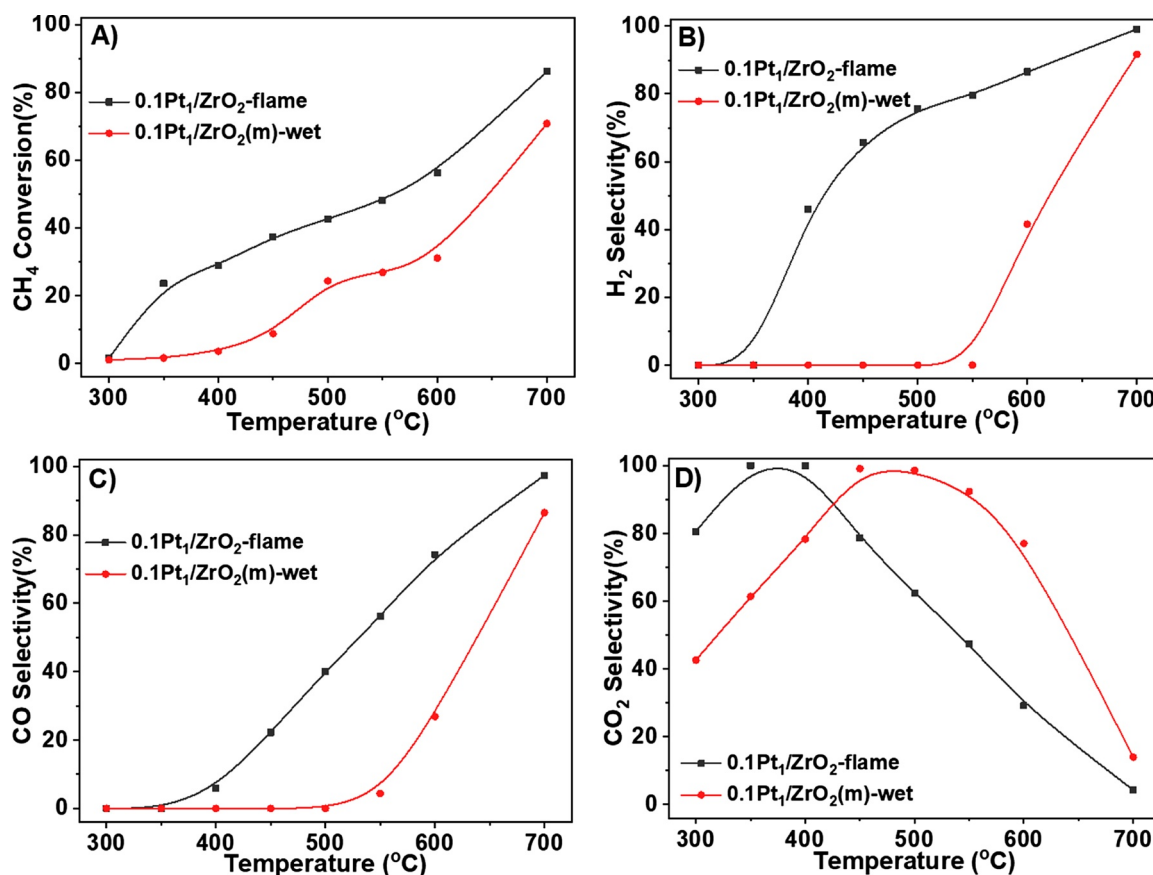


Fig. 7. (A) The methane conversion, (B) H₂ selectivity, (C) CO selectivity, and (D) CO₂ selectivity on 0.1Pt₁/ZrO₂-flame and 0.1Pt₁/ZrO₂(m)-wet in methane partial oxidation reaction. Reaction conditions: 3.33 % methane, 1.67 % O₂, balance Ar with a total flow rate of 30 mL/min, 30 mg of catalysts.

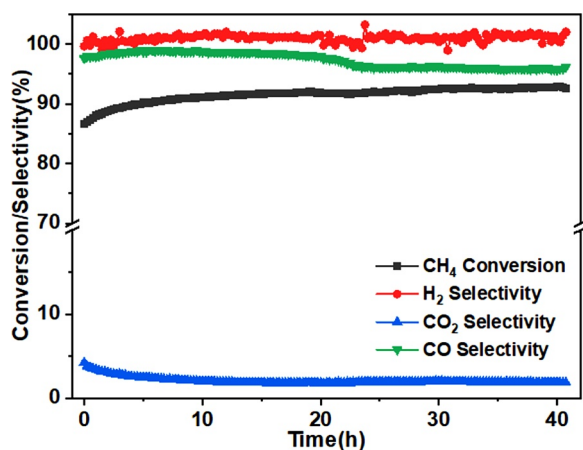


Fig. 8. Methane conversion, H₂ selectivity, CO selectivity and CO₂ selectivity over single-atom 0.1Pt₁/ZrO₂-flame for methane partial oxidation during the long-term stability test. Reaction conditions: 3.33 % methane, 1.67 % O₂, balance Ar with a total flow rate of 30 mL/min, 30 mg of catalysts, 700 °C.

supervised the project. S.D. and N.Y. designed the experiments, analyzed the data, and wrote the manuscript. O.M. and J.P. carried out catalyst synthesis and BET characterizations. S.D., M.H., and X.F. evaluated the catalytic performances and conducted some characterizations. H.C. and C.Y. conducted X-ray experiments in the synchrotron facility, and analysed the data. Q.H. performed HAADF-STEM analysis. All authors discussed the results and edited the manuscript.

Declaration of Competing Interest

The authors report no declarations of interest.

Acknowledgments

This work is supported by the National University of Singapore Flagship Green Energy Program (#R-279-000-553-646 and R-279-000-553-731). The authors are grateful for the Basic Research Grant from the Thailand Science Research and Innovation (BRG61-Joongjai Panpranot) and the Ratchadapisek Sompoch Endowment Fund from Chulalongkorn University. HAC and CMY acknowledge the financial supports from the Ministry of Science and Technology in Taiwan under the contracts No. MOST 106-2113-M-007-025-MY3 and MOST 107-3017-F-007-002 and the support by the Frontier Research Center on Fundamental and Applied Sciences of Matters from The Featured Areas Research Center Program within the framework of the Higher Education Sprout Project by the Ministry of Education (MOE) in Taiwan. National Synchrotron Radiation Research Centre (NSRRC) of Taiwan is gratefully acknowledged for XAS measurements.

Appendix A. Supplementary data

Supplementary material related to this article can be found, in the online version, at doi:<https://doi.org/10.1016/j.apcatb.2020.119471>.

References

- [1] B. Qiao, A. Wang, X. Yang, L.F. Allard, Z. Jiang, Y. Cui, J. Liu, J. Li, T. Zhang, Single-atom catalysis of CO oxidation using Pt₁/FeO_x, Nat. Chem. 3 (8) (2011) 634–641.
- [2] M. Flytzani-Stephanopoulos, B.C. Gates, Atomically dispersed supported metal

- catalysts, *Annu. Rev. Chem. Biomol. Eng.* 3 (1) (2012) 545–574.
- [3] A. Wang, J. Li, T. Zhang, Heterogeneous single-atom catalysis, *Int. Rev. Chem. Eng.* 2 (6) (2018) 65–81.
- [4] Z. Li, S. Ji, Y. Liu, X. Cao, S. Tian, Y. Chen, Z. Niu, Y. Li, Well-defined materials for heterogeneous catalysis: from nanoparticles to isolated single-atom sites, *Chem. Rev.* 120 (2) (2020) 623–682.
- [5] Y. Chen, S. Ji, C. Chen, Q. Peng, D. Wang, Y. Li, Single-atom catalysts: synthetic strategies and electrochemical applications, *Joule* 2 (7) (2018) 1242–1264.
- [6] L. Liu, A. Corma, Metal catalysts for heterogeneous catalysis: from single atoms to nanoclusters and nanoparticles, *Chem. Rev.* 118 (10) (2018) 4981–5079.
- [7] X. Cui, W. Li, P. Ryabchuk, K. Junge, M. Beller, Bridging homogeneous and heterogeneous catalysis by heterogeneous single-metal-site catalysts, *Nat. Catal.* 1 (6) (2018) 385–397.
- [8] S. Ding, M.J. Hülsey, J. Pérez-Ramírez, N. Yan, Transforming energy with single-atom catalysts, *Joule* 3 (12) (2019) 2897–2929.
- [9] S. Ding, Y. Guo, M.J. Hülsey, B. Zhang, H. Asakura, L. Liu, Y. Han, M. Gao, J.-y. Hasegawa, B. Qiao, T. Zhang, N. Yan, Electrostatic stabilization of single-atom catalysts by ionic liquids, *Chem* 5 (12) (2019) 3207–3219.
- [10] N. Yi, R. Si, H. Saltsburg, M. Flytzani-Stephanopoulos, Fuels of the future, *Energy Environ. Sci.* 3 (3) (2010) 831–837.
- [11] N. Yi, H. Saltsburg, M. Flytzani-Stephanopoulos, Hydrogen production by dehydrogenation of formic acid on atomically dispersed gold on ceria, *ChemSuschem* 6 (5) (2013) 816–819.
- [12] S.K. Kaiser, E. Fako, G. Manzocchi, F. Krumeich, R. Hauert, A.H. Clark, O.V. Safonova, N. Lopez, J. Perez-Ramirez, Nanostructuring unlocks high performance of platinum single-atom catalysts for stable vinyl chloride production, *Nat. Catal.* 3 (4) (2020) 376–385.
- [13] E. Vorobyeva, E. Fako, Z. Chen, S.M. Collins, D. Johnstone, P.A. Midgley, R. Hauert, O.V. Safonova, G. Vile, N. Lopez, S. Mitchell, J. Perez-Ramirez, Atom-by-Atom resolution of structure-function relations over low-nuclearity metal catalysts, *Angew. Chem. Int. Ed.* 58 (26) (2019) 8724–8729.
- [14] Z. Chen, S. Mitchell, F. Krumeich, R. Hauert, S. Yakunin, M.V. Kovalenko, J. Pérez-Ramírez, Tunability and scalability of single-atom catalysts based on carbon nitride, *ACS Sustain. Chem. Eng.* 7 (5) (2019) 5223–5230.
- [15] S. Liu, L. Bai, A.P. van Muyden, Z. Huang, X. Cui, Z. Fei, X. Li, X. Hu, P.J. Dyson, Oxidative cleavage of β -O-4 bonds in lignin model compounds with a single-atom Co catalyst, *Green Chem.* 21 (8) (2019) 1974–1981.
- [16] Y. Ma, B. Chi, W. Liu, L. Cao, Y. Lin, X. Zhang, X. Ye, S. Wei, J. Lu, Tailoring of the proximity of platinum single atoms on CeO₂ using phosphorus boosts the hydrogenation activity, *ACS Catal.* 9 (9) (2019) 8404–8412.
- [17] J. Li, Q. Guan, H. Wu, W. Liu, Y. Lin, Z. Sun, X. Ye, X. Zheng, H. Pan, J. Zhu, S. Chen, W. Zhang, S. Wei, J. Lu, Highly active and stable metal single-atom catalysts achieved by strong electronic metal-support interactions, *J. Am. Chem. Soc.* 141 (37) (2019) 14515–14519.
- [18] L. Cao, W. Liu, Q. Luo, R. Yin, B. Wang, J. Weissenrieder, M. Soldemo, H. Yan, Y. Lin, Z. Sun, C. Ma, W. Zhang, S. Chen, H. Wang, Q. Guan, T. Yao, S. Wei, J. Yang, J. Lu, Atomically dispersed iron hydroxide anchored on Pt for preferential oxidation of CO in H₂, *Nature* 565 (7741) (2019) 631–635.
- [19] X. He, Y. Deng, Y. Zhang, Q. He, D. Xiao, M. Peng, Y. Zhao, H. Zhang, R. Luo, T. Gan, H. Ji, D. Ma, Mechanochemical kilogram-scale synthesis of noble metal single-atom catalysts, *Cell Rep. Phys. Sci.* 1 (1) (2020).
- [20] L. Lin, S. Yao, R. Gao, X. Liang, Q. Yu, Y. Deng, J. Liu, M. Peng, Z. Jiang, S. Li, Y.W. Li, X.D. Wen, W. Zhou, D. Ma, A highly CO-tolerant atomically dispersed Pt catalyst for chemoselective hydrogenation, *Nat. Nanotechnol.* 14 (4) (2019) 354–361.
- [21] F. Huang, Y. Deng, Y. Chen, X. Cai, M. Peng, Z. Jia, P. Ren, D. Xiao, X. Wen, N. Wang, H. Liu, D. Ma, Atomically dispersed Pd on nanodiamond/graphene hybrid for selective hydrogenation of acetylene, *J. Am. Chem. Soc.* 140 (41) (2018) 13142–13146.
- [22] H. Xu, N. Jiang, D. Wang, L. Wang, Y. Song, Z. Chen, J. Ma, T. Zhang, Improving PMS oxidation of organic pollutants by single cobalt atom catalyst through hybrid radical and non-radical pathways, *Appl. Catal. B* (2020) 263.
- [23] X. Lv, W. Wei, H. Wang, B. Huang, Y. Dai, Holey graphitic carbon nitride (g-CN) supported bifunctional single atom electrocatalysts for highly efficient overall water splitting, *Appl. Catal. B* (2020) 264.
- [24] W. Zhu, J. Fu, J. Liu, Y. Chen, X. Li, K. Huang, Y. Cai, Y. He, Y. Zhou, D. Su, J.-J. Zhu, Y. Lin, Tuning single atom-nanoparticle ratios of Ni-based catalysts for synthesis gas production from CO₂, *Appl. Catal. B* (2020) 264.
- [25] S. Cao, M. Yang, A.O. Elnabawy, A. Trimpalis, S. Li, C. Wang, F. Goltz, Z. Chen, J. Liu, J. Shan, M. Li, T. Haas, K.W. Chapman, S. Lee, L.F. Allard, M. Mavrikakis, M. Flytzani-Stephanopoulos, Single-atom gold oxo-clusters prepared in alkaline solutions catalyze the heterogeneous methanol self-coupling reactions, *Nat. Chem.* 11 (12) (2019) 1098–1105.
- [26] X. Zhong, W. Yi, Y. Qu, L. Zhang, H. Bai, Y. Zhu, J. Wan, S. Chen, M. Yang, L. Huang, M. Gu, H. Pan, B. Xu, Co single-atom anchored on Co₃O₄ and nitrogen-doped active carbon toward bifunctional catalyst for zinc-air batteries, *Appl. Catal. B* (2020) 260.
- [27] M.J. Hülsey, J. Zhang, N. Yan, Harnessing the wisdom in colloidal chemistry to make stable single-atom catalysts, *Adv. Mater.* 30 (47) (2018) e1802304.
- [28] J.-C. Liu, Y. Tang, Y.-G. Wang, T. Zhang, J. Li, Theoretical understanding of the stability of single-atom catalysts, *Sci. Rev.* 5 (5) (2018) 638–641.
- [29] R. Lang, W. Xi, J.C. Liu, Y.T. Cui, T. Li, A.F. Lee, F. Chen, Y. Chen, L. Li, L. Li, J. Lin, S. Miao, X. Liu, A.Q. Wang, X. Wang, J. Luo, B. Qiao, J. Li, T. Zhang, Non defect-stabilized thermally stable single-atom catalyst, *Nat. Commun.* 10 (1) (2019) 234.
- [30] B. Zhang, G. Sun, S. Ding, H. Asakura, J. Zhang, P. Sautet, N. Yan, Atomically dispersed Pt₁-polyoxometalate catalysts: how does metal-support interaction affect stability and hydrogenation activity? *J. Am. Chem. Soc.* 141 (20) (2019) 8185–8197.
- [31] Y. Ren, Y. Tang, L. Zhang, X. Liu, L. Li, S. Miao, D. Sheng Su, A. Wang, J. Li, T. Zhang, Unraveling the coordination structure-performance relationship in Pt₁/Fe₂O₃ single-atom catalyst, *Nat. Commun.* 10 (1) (2019) 4500.
- [32] J. Zhang, X. Wu, W.C. Cheong, W. Chen, R. Lin, J. Li, L. Zheng, W. Yan, L. Gu, C. Chen, Q. Peng, D. Wang, Y. Li, Cation vacancy stabilization of single-atomic-site Pt₁/Ni(OH)_x catalyst for diboration of alkynes and alkenes, *Nat. Commun.* 9 (1) (2018) 1002.
- [33] L. Lin, W. Zhou, R. Gao, S. Yao, X. Zhang, W. Xu, S. Zheng, Z. Jiang, Q. Yu, Y.W. Li, C. Shi, X.D. Wen, D. Ma, Low-temperature hydrogen production from water and methanol using Pt/alpha-MoC catalysts, *Nature* 544 (7648) (2017) 80–83.
- [34] J. Shan, M. Li, L.F. Allard, S. Lee, M. Flytzani-Stephanopoulos, Mild oxidation of methane to methanol or acetic acid on supported isolated rhodium catalysts, *Nature* 551 (7682) (2017) 605–608.
- [35] M. Yang, J. Liu, S. Lee, B. Zucig, J. Huang, L.F. Allard, M. Flytzani-Stephanopoulos, A common single-site Pt(II)-O(OH)_x species stabilized by sodium on "active" and "inert" supports catalyzes the water-gas shift reaction, *J. Am. Chem. Soc.* 137 (10) (2015) 3470–3473.
- [36] Y. Tang, C. Asokan, M. Xu, G.W. Graham, X. Pan, P. Christopher, J. Li, P. Sautet, Rh single atoms on TiO₂ dynamically respond to reaction conditions by adapting their site, *Nat. Commun.* 10 (1) (2019) 4488.
- [37] L. DeRita, S. Dai, K. Lopez-Zepeda, N. Pham, G.W. Graham, X. Pan, P. Christopher, Catalyst architecture for stable single atom dispersion enables site-specific spectroscopic and reactivity measurements of CO Adsorbed to Pt atoms, oxidized Pt clusters, and metallic Pt clusters on TiO₂, *J. Am. Chem. Soc.* 139 (40) (2017) 14150–14165.
- [38] H. Fei, J. Dong, Y. Feng, C.S. Allen, C. Wan, B. Voloskiy, M. Li, Z. Zhao, Y. Wang, H. Sun, P. An, W. Chen, Z. Guo, C. Lee, D. Chen, I. Shakir, M. Liu, T. Hu, Y. Li, A.I. Kirkland, X. Duan, Y. Huang, General synthesis and definitive structural identification of MN₄C₄ single-atom catalysts with tunable electrocatalytic activities, *Nat. Catal.* 1 (1) (2018) 63–72.
- [39] Y. Yao, Z. Huang, P. Xie, L. Wu, L. Ma, T. Li, Z. Pang, M. Jiao, Z. Liang, J. Gao, Y. He, D.J. Kline, M.R. Zachariah, C. Wang, J. Lu, T. Wu, T. Li, C. Wang, R. Shahbazian-Yassar, L. Hu, High temperature shockwave stabilized single atoms, *Nat. Nanotechnol.* 14 (9) (2019) 851–857.
- [40] J. Jones, H. Xiong, A.T. DeLaRiva, E.J. Peterson, H. Pham, S.R. Challa, G. Qi, S. Oh, M.H. Wiebenga, X.I. Pereira Hernandez, Y. Wang, A.K. Datye, Thermally stable single-atom platinum-on-ceria catalysts via atom trapping, *Science* 353 (6295) (2016) 150–154.
- [41] S. Wei, A. Li, J.C. Liu, Z. Li, W. Chen, Y. Gong, Q. Zhang, W.C. Cheong, Y. Wang, L. Zheng, H. Xiao, C. Chen, D. Wang, Q. Peng, L. Gu, X. Han, J. Li, Y. Li, Direct observation of noble metal nanoparticles transforming to thermally stable single atoms, *Nat. Nanotechnol.* 13 (9) (2018) 856–861.
- [42] H. Zhou, Y. Zhao, J. Xu, H. Sun, Z. Li, W. Liu, T. Yuan, W. Liu, X. Wang, W.C. Cheong, Z. Wang, X. Wang, C. Zhao, Y. Yao, W. Wang, F. Zhou, M. Chen, B. Jin, R. Sun, J. Liu, X. Hong, T. Yao, S. Wei, J. Luo, Y. Wu, Recover the activity of sintered supported catalysts by nitrogen-doped carbon atomization, *Nat. Commun.* 11 (1) (2020) 335.
- [43] K. Liu, X. Zhao, G. Ren, T. Yang, Y. Ren, A.F. Lee, Y. Su, X. Pan, J. Zhang, Z. Chen, J. Yang, X. Liu, T. Zhou, W. Xi, J. Luo, C. Zeng, H. Matsumoto, W. Liu, Q. Jiang, K. Wilson, A. Wang, B. Qiao, W. Li, T. Zhang, Strong metal-support interaction promoted scalable production of thermally stable single-atom catalysts, *Nat. Commun.* 11 (1) (2020) 1263.
- [44] D. Kunwar, S. Zhou, A. DeLaRiva, E.J. Peterson, H. Xiong, X.I. Pereira-Hernández, S.C. Purdy, R. ter Veen, H.H. Brongersma, J.T. Miller, H. Hashiguchi, L. Kovarik, S. Lin, H. Guo, Y. Wang, A.K. Datye, Stabilizing high metal loadings of thermally stable platinum single atoms on an industrial catalyst support, *ACS Catal.* 9 (5) (2019) 3978–3990.
- [45] T. Rudin, K. Wegner, S.E. Pratsinis, Uniform nanoparticles by flame-assisted spray pyrolysis (FASP) of low cost precursors, *J. Nanopart. Res.* 13 (7) (2011) 2715–2725.
- [46] B. Pongthawornsakun, O. Mekasuwandumrong, S. Prakash, E. Ehret, F.J.C. Santos Aires, J. Panpranot, Effect of reduction temperature on the characteristics and catalytic properties of TiO₂ supported AuPd alloy particles prepared by one-step flame spray pyrolysis in the selective hydrogenation of 1-heptyne, *Appl. Catal. A Gen.* 506 (2015) 278–287.
- [47] K.A. Michalow-Mauke, Y. Lu, K. Kowalski, T. Graule, M. Nachttegaal, O. Kröcher, D. Ferri, Flame-made WO₃/CeO_x-TiO₂ Catalysts for selective catalytic reduction of NO_x by NH₃, *ACS Catal.* 5 (10) (2015) 5657–5672.
- [48] D. Nunes, A.P.L. Santos, L. PedroBarquinha; Pereira, E. Fortunato, R. Martins, Synthesis, design, and morphology of metal oxide nanostructures, *Metal Oxide Nanostructures, Synthesis, Properties and Applications*, Elsevier, 2019, p. P33.
- [49] T.V. Gavrilović, D.J. Jovanović, M.D. Dramićanin, *Nanomaterials for Green Energy*, Elsevier, 2018.
- [50] R. Strobel, Flame spray synthesis of Pd/Al₂O₃ catalysts and their behavior in enantioselective hydrogenation, *J. Catal.* 222 (2) (2004) 307–314.
- [51] G. Chiarello, I. Rossetti, L. Forni, Flame-spray pyrolysis preparation of perovskites for methane catalytic combustion, *J. Catal.* 236 (2) (2005) 251–261.
- [52] R. Strobel, S.E. Pratsinis, A. Baiker, Flame-made Pd/La₂O₃/Al₂O₃ nanoparticles: thermal stability and catalytic behavior in methane combustion, *J. Mater. Chem.* 15 (5) (2005).
- [53] K. Schuh, W. Kleist, M. Høj, V. Trouillet, A.D. Jensen, J.D. Grunwaldt, One-step synthesis of bismuth molybdate catalysts via flame spray pyrolysis for the selective oxidation of propylene to acrolein, *Chem. Commun.* 50 (97) (2014) 15404–15406.
- [54] S. Pisdungdaw, J. Panpranot, C. Methastidsook, C. Chaisuk, K. Faungnawakij, P. Praserttham, O. Mekasuwandumrong, Characteristics and catalytic properties of

- Pt–Sn/Al₂O₃ nanoparticles synthesized by one-step flame spray pyrolysis in the dehydrogenation of propane, *Appl. Catal. A Gen.* 370 (1–2) (2009) 1–6.
- [55] K. Fujiwara, S.E. Pratsinis, Single Pd atoms on TiO₂ dominate photocatalytic NO_x removal, *Appl. Catal. B* 226 (2018) 127–134.
- [56] K. Fujiwara, S.E. Pratsinis, Atomically dispersed Pd on nanostructured TiO₂ for NO removal by solar light, *AlChE J.* 63 (1) (2017) 139–146.
- [57] C.-H. Wang, C.-W. Su, S.W. Chan, L.-J. Fan, M.-C. Chen, Y.-W. Yang, Damaging effect of hot metal atoms on organic semiconducting films during top contact formation, *J. Phys. Chem. C* 119 (26) (2015) 14593–14602.
- [58] A. Jentys, Estimation of mean size and shape of small metal particles by EXAFS, *Phys. Chem. Chem. Phys.* 1 (17) (1999) 4059–4063.
- [59] C.-m. Yang, P.-h. Liu, Y.-f. Ho, C.-y. Chiu, K.-j. Chao, Highly dispersed metal nanoparticles in functionalized SBA-15, *Chem. Mater.* 15 (1) (2003) 275–280.
- [60] X. Li, H. Rong, J. Zhang, D. Wang, Y. Li, Modulating the local coordination environment of single-atom catalysts for enhanced catalytic performance, *Nano Res.* 13 (7) (2020).
- [61] Q. Xu, C. Guo, S. Tian, J. Zhang, W. Chen, W.-C. Cheong, L. Gu, L. Zheng, J. Xiao, Q. Liu, B. Li, D. Wang, Y. Li, Coordination structure dominated performance of single-atomic Pt catalyst for anti-Markovnikov hydroboration of alkenes, *Sci. China Mater.* 63 (6) (2020) 972–981.
- [62] Z. Zhang, Y. Zhu, H. Asakura, B. Zhang, J. Zhang, M. Zhou, Y. Han, T. Tanaka, A. Wang, T. Zhang, N. Yan, Thermally stable single atom Pt/m-Al₂O₃ for selective hydrogenation and CO oxidation, *Nat. Commun.* 8 (2017) 16100.
- [63] J. van Bokhoven, Recent developments in X-ray absorption spectroscopy, *Phys. Chem. Chem. Phys.* 12 (21) (2010) 5502.
- [64] R.D. Shannon, Revised effective ionic radii and systematic studies of interatomic distances in halides and chalcogenides, *Acta Crystallogr. Sect. A: Found. Crystallogr.* 32 (5) (1976) 751–767.
- [65] B.M. Weckhuysen, I.E. Wachs, *Handbook of Surfaces and Interfaces of Materials*, Chapter 11, Catalysis by Supported Metal Oxides, 2001.
- [66] G. Hilson, A.J. Monhemius, Alternatives to cyanide in the gold mining industry: what prospects for the future? *J. Cleaner Prod.* 14 (12–13) (2006) 1158–1167.
- [67] C. Wang, G. Garbarino, L.F. Allard, F. Wilson, G. Busca, M. Flytzani-Stephanopoulos, Low-temperature dehydrogenation of ethanol on atomically dispersed gold supported on ZnZrO_x, *ACS Catal.* 6 (1) (2015) 210–218.
- [68] Y. Guan, E.J. Hensen, Cyanide leaching of Au/CeO₂: highly active gold clusters for 1,3-butadiene hydrogenation, *Phys. Chem. Chem. Phys.* 11 (41) (2009) 9578–9582.
- [69] Q. Fu, H. Saltsburg, M. Flytzani-Stephanopoulos, Active nonmetallic Au and Pt species on ceria-based water-gas shift catalysts, *Science* 301 (5635) (2003) 935–938.
- [70] C.J. Howard, R.J. Hill, B.E. Reichert, Structures of ZrO₂ polymorphs at room temperature by high-resolution neutron powder diffraction, *Acta Crystallogr. B* 44 (1988) 116–120.
- [71] P. Bouvier, E. Djurado, C. Ritter, A.J. Dianoux, G. Lucazeau, Low temperature phase transformation of nanocrystalline tetragonal ZrO₂ by neutron and Raman scattering studies, *Int. J. Inorg. Mater.* 3 (2001) 647–654.
- [72] S. Grazulis, D. Chateigner, R.T. Downs, A.T. Yokochi, M. Quiros, L. Lutterotti, E. Manakova, J. Butkus, P. Moeck, A. Le Bail, *Crystallography Open Database – an open-access collection of crystal structures*, *J. Appl. Cryst.* 42 (2009) 726–729.
- [73] M.J. Hulsey, B. Zhang, Z. Ma, H. Asakura, D.A. Do, W. Chen, T. Tanaka, P. Zhang, Z. Wu, N. Yan, In situ spectroscopy-guided engineering of rhodium single-atom catalysts for CO oxidation, *Nat. Commun.* 10 (1) (2019) 1330.
- [74] L. DeRita, J. Resasco, S. Dai, A. Boubnov, H.V. Thang, A.S. Hoffman, I. Ro, G.W. Graham, S.R. Bare, G. Pacchioni, X. Pan, P. Christopher, Structural evolution of atomically dispersed Pt catalysts dictates reactivity, *Nat. Mater.* 18 (7) (2019) 746–751.
- [75] J. Resasco, L. DeRita, S. Dai, J.P. Chada, M. Xu, X. Yan, J. Finzel, S. Hanukovich, A.S. Hoffman, G.W. Graham, S.R. Bare, X. Pan, P. Christopher, Uniformity is key in defining structure-function relationships for atomically dispersed metal catalysts: the case of Pt/CeO₂, *J. Am. Chem. Soc.* 142 (1) (2020) 169–184.
- [76] J. Andersson, M. Antonsson, L. Eurenus, E. Olsson, M. Skoglundh, Deactivation of diesel oxidation catalysts: vehicle- and synthetic aging correlations, *Appl. Catal. B* 72 (1–2) (2007) 71–81.
- [77] L. Nie, D. Mei, H. Xiong, B. Peng, Z. Ren, X.L.P. Hernandez, A. DeLaRiva, M. Wang, M.H. Engelhard, L. Kovarik, A.K. Datye, Y. Wang, Activation of surface lattice oxygen in single-atom Pt/CeO₂ for low-temperature CO oxidation, *Science* 358 (6369) (2017) 1419–1423.
- [78] X. Zhou, Q. Shen, K. Yuan, W. Yang, Q. Chen, Z. Geng, J. Zhang, X. Shao, W. Chen, G. Xu, X. Yang, K. Wu, Unraveling charge state of supported Au single-atoms during CO oxidation, *J. Am. Chem. Soc.* 140 (2) (2018) 554–557.
- [79] A.J. Therrien, A.J.R. Hensley, M.D. Marcinkowski, R. Zhang, F.R. Lucci, B. Coughlin, A.C. Schilling, J.-S. McEwen, E.C.H. Sykes, An atomic-scale view of single-site Pt catalysis for low-temperature CO oxidation, *Nat. Catal.* 1 (3) (2018) 192–198.
- [80] B. Han, T. Li, J. Zhang, C. Zeng, H. Matsumoto, Y. Su, B. Qiao, T. Zhang, A highly active Rh1/CeO₂ single-atom catalyst for low-temperature CO oxidation, *Chem. Commun.* 56 (36) (2020) 4870–4873.
- [81] B. Han, R. Lang, H. Tang, J. Xu, X.-K. Gu, B. Qiao, J. Liu, Superior activity of Rh1/ZnO single-atom catalyst for CO oxidation, *Chin. J. Catal.* 40 (12) (2019) 1847–1853.
- [82] X. Yang, X. Yu, M. Lin, M. Ge, Y. Zhao, F. Wang, Interface effect of mixed phase Pt/ZrO₂ catalysts for HCHO oxidation at ambient temperature, *J. Mater. Chem. A* 5 (26) (2017) 13799–13806.
- [83] C. Gao, J. Low, R. Long, T. Kong, J. Zhu, Y. Xiong, Heterogeneous single-atom photocatalysts: fundamentals and applications, *Chem. Rev.* (2020) doi:https://doi.org/10.1021/acs.chemrev.9b00840.
- [84] X. Guo, G. Fang, G. Li, H. Ma, H. Fan, L. Yu, C. Ma, X. Wu, D. Deng, M. Wei, D. Tan, R. Si, S. Zhang, J. Li, L. Sun, Z. Tang, X. Pan, X. Bao, Direct, nonoxidative conversion of methane to ethylene, aromatics, and hydrogen, *Science* 344 (6184) (2014) 616–619.
- [85] L. He, Y. Fan, J. Bellettre, J. Yue, L. Luo, A review on catalytic methane combustion at low temperatures: catalysts, mechanisms, reaction conditions and reactor designs, *Renew. Sustain. Energy Rev.* (2020) 119.
- [86] J. Yang, Y. Guo, Nanostructured perovskite oxides as promising substitutes of noble metals catalysts for catalytic combustion of methane, *Chin. Chem. Lett.* 29 (2) (2018) 252–260.
- [87] V. Bashan, Y. Ust, Perovskite catalysts for methane combustion: applications, design, effects for reactivity and partial oxidation, *Int. J. Energy Res.* 43 (2019) 7755–7789.
- [88] T.V. Choudhary, S. Banerjee, V.R. Choudhary, Catalysts for combustion of methane and lower alkanes, *Appl. Catal. A Gen.* 234 (1–2) (2002) 1–23.
- [89] W. Li, H. Huang, H. Li, W. Zhang, H. Liu, Facile synthesis of pure monoclinic and tetragonal zirconia nanoparticles and their phase effects on the behavior of supported molybdena catalysts for methanol-selective oxidation, *Langmuir* 24 (15) (2008) 8358–8366.
- [90] Z. Xu, Y. Yue, X. Bao, Z. Xie, H. Zhu, Propane dehydrogenation over Pt clusters localized at the Sn single-site in zeolite framework, *ACS Catal.* 10 (1) (2019) 818–828.
- [91] D. Neumann, Gt. Veser, Catalytic partial oxidation of methane in a high-temperature reverse-flow reactor, *AlChE J.* 51 (1) (2005) 210–223.
- [92] M. Akri, S. Zhao, X. Li, K. Zang, A.F. Lee, M.A. Isaacs, W. Xi, Y. Gangarajula, J. Luo, Y. Ren, Y.T. Cui, L. Li, Y. Su, X. Pan, W. Wen, Y. Pan, K. Wilson, L. Li, B. Qiao, H. Ishii, Y.F. Liao, A. Wang, X. Wang, T. Zhang, Atomically dispersed nickel as coke-resistant active sites for methane dry reforming, *Nat. Commun.* 10 (1) (2019) 5181.